



*Citation for published version:*

Ajaereh, MGO, Cook, OJ, Jones, HN, Kizer, N, Katch, L, Wheatley, CS, Vagg, C, Courtney, C, Kube, CM, Argüelles, AP & Ajaereh, MGO 2024, Assessing spatial non-uniformities in lithium-ion battery state of charge using ultrasound immersion testing. in *Proceedings of Meetings on Acoustics*. 1 edn, vol. 54, 3aPAb8, Proceedings of Meetings on Acoustics, Acoustical Society of America, Ottawa, Ontario, Canada, pp. 1-13, 186th Meeting of the Acoustical Society of America and the Canadian Acoustical Association, Ontario, Canada, 13/05/24. <https://doi.org/10.1121/2.0001950>, <https://doi.org/10.1121/2.0001950>

*DOI:*

[10.1121/2.0001950](https://doi.org/10.1121/2.0001950)

[10.1121/2.0001950](https://doi.org/10.1121/2.0001950)

*Publication date:*

2024

*Document Version*

Publisher's PDF, also known as Version of record

[Link to publication](#)

**University of Bath**

**Alternative formats**

If you require this document in an alternative format, please contact:  
[openaccess@bath.ac.uk](mailto:openaccess@bath.ac.uk)

**General rights**




Copyright and moral rights for the publications made accessible in the public portal are retained by the authors and/or other copyright owners and it is a condition of accessing publications that users recognise and abide by the legal requirements associated with these rights.

**Take down policy**

If you believe that this document breaches copyright please contact us providing details, and we will remove access to the work immediately and investigate your claim.

SEPTEMBER 13 2024

## Assessing spatial non-uniformities in lithium-ion battery state of charge using ultrasound immersion testing

Mac Geoffrey Obinna Ajaereh ; Olivia J. Cook; Haley N. Jones; Nathan Kizer; Lauren Katch; Christopher S. Wheatley, Jr.; Christopher Vagg; Charles Courtney; Christopher M. Kube ; Andrea P. Argüelles 



*Proc. Mtgs. Acoust.* 54, 045004 (2024)

<https://doi.org/10.1121/2.0001950>



**ASA**

Advance your science and career as a member of the  
**Acoustical Society of America**

[LEARN MORE](#)



**ASA**  
ACOUSTICAL SOCIETY  
OF AMERICA



*Acoustics Week in Canada*

**Joint Meeting  
186th Meeting of the Acoustical Society of America  
and the Canadian Acoustical Association**

Ottawa, Ontario, Canada  
13-17 May 2024

**Physical Acoustics: Paper 3aPAb8**

**Assessing spatial non-uniformities in lithium-ion battery state of charge using ultrasound immersion testing**

**Mac Geoffrey Obinna Ajaereh**

*Department of Mechanical Engineering, University of Bath Faculty of Engineering and Design, Bath, Somerset, BA2 7AY, UNITED KINGDOM; mgoa20@bath.ac.uk*

**Olivia J. Cook**

*Department of Engineering Science and Mechanics, The Pennsylvania State University, State College, PA, 16802; ojc3@psu.edu*

**Haley N. Jones**

*Department of Materials Science and Engineering, The Pennsylvania State University, State College, PA, 16802; hnj5051@psu.edu*

**Nathan Kizer, Lauren Katch and Christopher S. Wheatley Jr.**

*Department of Engineering Science and Mechanics, The Pennsylvania State University, State College, PA, 16802; njk19@psu.edu; luk50@psu.edu; cs.wheatleyjr@psu.edu*

**Christopher Vagg and Charles Courtney**

*Department of Mechanical Engineering, University of Bath Faculty of Engineering and Design, Bath, Somerset, BA2 7AY, UNITED KINGDOM; C.R.M.Vagg@bath.ac.uk; C.R.P.Courtney@bath.ac.uk*

**Christopher M. Kube and Andrea P. Argüelles**

*Department of Engineering Science and Mechanics, The Pennsylvania State University, State College, PA, 16802; kube@psu.edu; arguelles@psu.edu*

Enhancing the performance, safety and reliability of battery management systems is crucial for advancing the state of the art in battery electric vehicles. Current research explores the potential of ultrasound to monitor state of charge (SoC) changes in individual batteries. Understanding spatial variations in SoC is essential, as non-uniformities could lead to sub-optimal performance, premature aging, and possible safety risks. This study uses ultrasound immersion testing to map wave speed and attenuation at different SoC levels during battery discharging. Results indicate non-uniform wave speed and attenuation suggestive of SoC spatial variations within single cells. Future work will include acoustic measurements under various discharge rates and relaxation periods to provide further insights into SoC inhomogeneities. Potential causes of structure and manufacturing variations of the battery are discussed, highlighting the need to address these issues to prevent over-charging/over-discharging in specific battery areas.



## 1. INTRODUCTION

Electric vehicles (EVs) are crucial for addressing the impact of road transport on health, climate, and the environment (Zhang and Fujimori (2020)). Lithium-ion (Li-ion) batteries, known for their high power, energy density, long lifespan, and eco-friendliness, are widely used in EVs and energy storage systems (Jaguemont et al. (2016)). However, automotive batteries face issues like safety, durability, and cost. Over-charging or over-discharging can lead to fire risks due to thermal runaway, where temperature increases uncontrollably (Ghiji et al. (2020), Lu et al. (2013), and Q. Wang et al. (2019)), posing dangers to passengers. Extreme charging can cause dendrite growth, leading to local heating and affecting neighbouring cells (Liao et al. (2019), Tran et al. (2022), and Xu et al. (2021)).

Batteries can release hazardous chemicals and gases that are hard to detect, and although EV fires are rare, they are serious (Hassan et al. (2023) and Hynynen et al. (2023)). Accurate State of Charge (SoC) estimations are essential for safe, efficient, and reliable battery systems, and they also provide a crucial motivation for assessing the state of health (SoH) of batteries. The SoC of a Li-ion battery indicates the available charge capacity, ranging from 0% (empty) to 100% (full) (Hannan et al. (2017)). Common SoC estimation techniques include Coulomb counting and Open-Circuit Voltage (OCV) (Fathoni et al. (2017)). Coulomb counting integrates current over time to estimate capacity but can accumulate errors due to losses and self-discharge. OCV uses a discharge curve but is affected by temperature and electrochemical kinetics, and the measurements are often flat, making it difficult to accurately estimate SoC.

More recently, researchers at Princeton University proposed ultrasound non-destructive testing (NDT) proving to use it as an additional SoC tracking method (Hsieh et al. (2015)). This low-cost, non-invasive acoustic technique monitors changes in mechanical properties like density and elastic modulus to assess SoC. Combining ultrasound with methods such as Coulomb counting and OCV could improve SoC measurement reliability and battery safety (Davies et al. (2017)). SoC inhomogeneity in Li-ion batteries refers to the uneven distribution of charge, caused by factors such as cell manufacturing differences, aging, temperature variations, and usage patterns.

This uneven distribution can lead to local over-charge or over-discharge (Fang et al. (2017), Kehrwald et al. (2011), Lei et al. (2005), Maire et al. (2008), and Nanda et al. (2011)), potentially causing battery degradation (Cai et al. (2013) and Shao (2014)). SoC inhomogeneities have been studied using calorimetry (Maire et al. (2008)), neutron diffraction (Cai et al. (2013)), Raman spectroscopy (Fang et al. (2017), Lei et al. (2005), Migge et al. (2005), and Nanda et al. (2011)), scanning transmission X-ray microscopy (STXM) (Chueh et al. (2013)), and soft X-ray emission spectroscopy (Braun et al. (2010)). This work specifically aims to advance research in this field by understanding SoC inhomogeneities in lithium-polymer (Li-Po) batteries through ultrasound immersion testing. Although Li-Po batteries share a basic formulation with Li-ion batteries, they are distinguished by the use of a polymer electrolyte instead of a liquid electrolyte.

## 2. BACKGROUND

### A. STRUCTURE OF A LITHIUM POLYMER BATTERY

A standard Li-Po battery consists of two electrodes, known as the anode and the cathode, and an electrolyte system that facilitates the movement of ions between these electrodes as Figure 1.A shows (Long et al. (2016) and J. Wang et al. (2021)). The cathode is the positive electrode and typical choices of materials include layered  $LiMO_2$  (Mizushima et al. (1980)) ( $M = Mn, Co, \text{ and } Ni$ ), spinel  $LiMn_2O_4$  (Thackeray et al. (1983)), and olivine  $LiFePO_4$  (Padhi et al. (1997)). The anode is the negative electrode and is commonly made of graphite, forming a compound represented as  $LiC_6$ .

Li-Po batteries use solid or gel polymer electrolytes, such as those based on polyethylene oxide (PEO). These electrolytes enhance safety and flexibility but generally provide lower ionic conductivity compared

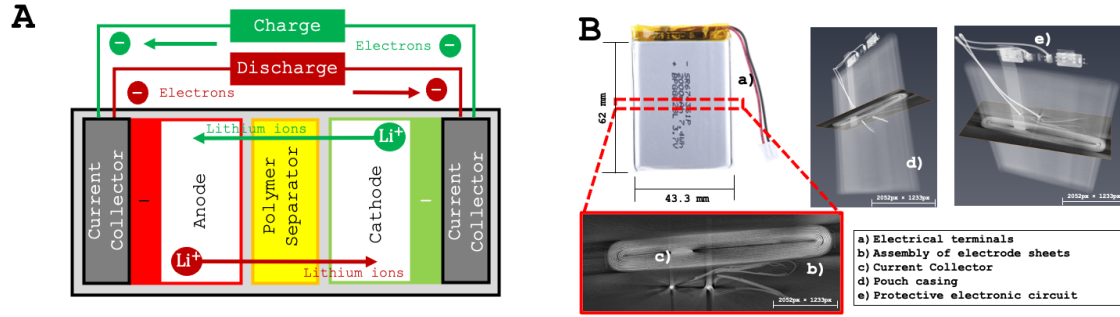


Figure 1: Structure of a Li-Po battery (A), and CT scan of the 3.7 V Li-Po battery used for all tests (B).

to liquid electrolytes. Additionally, the polymer electrolyte serves as both the electrolyte and the separator (Long et al. (2016)). During discharging, lithium ions migrate from the anode to the cathode through the polymer electrolyte, while electrons travel through the external circuit, providing electrical power. During charging, this process is reversed, with lithium ions moving back to the anode (Yang et al. (2020)).

## B. LONGITUDINAL WAVES IN ELASTIC SOLIDS

The speed of a longitudinal wave ( $c_{\text{longitudinal}}$ ) in an elastic solid depends on the properties of the medium (Hudson (1981)). For isotropic elastic materials, the wave speed is given by:

$$c_{\text{longitudinal}} = \sqrt{\frac{K + \frac{4}{3}G}{\rho}}, \quad (1)$$

where  $\rho$  is the density,  $K$  is the bulk modulus, and  $G$  is the shear modulus of the material. The bulk and shear modulus of the material are given by:

$$K = \frac{E}{3(1 - 2\nu)}, \quad (2)$$

$$G = \frac{E}{2(1 + \nu)}, \quad (3)$$

where  $E$  is the Young's modulus, and  $\nu$  is the Poisson's ratio. Both density and elastic moduli are crucial for SoC estimates. Acoustic impedance ( $Z$ ) is a property of the material and can be given by  $Z = \rho c_p$ . When an ultrasound wave travels through a material and reaches the boundary with another material, it interacts with this interface. The wave carries energy that must be conserved across the boundary. The degree of acoustic impedance mismatch between the two materials determines the proportion of the wave that is reflected versus transmitted. The larger the difference in impedance, the greater the reflection. This relationship is described by the reflection coefficient ( $R$ ) and the transmission coefficient ( $T$ ), which depend on the acoustic impedances of both materials for a normal incidence case:

$$R = \frac{Z_2 - Z_1}{Z_2 + Z_1}, \quad (4)$$

$$T = 1 - R, \quad (5)$$

where,  $Z_1$  and  $Z_2$  are the acoustic impedances of the first and second materials, respectively (Blitz and Simpson (1995), Messineo et al. (2016), and Nanekar and Shah (2003)). If the wave speeds of two materials are nearly equal,  $R$  approaches zero, indicating minimal reflection, and  $T$  approaches 1, indicating nearly complete transmission. Conversely, if wave speeds differ significantly,  $R$  increases, indicating more reflection, and  $T$  decreases, indicating less transmission.

### 3. METHODOLOGY

#### A. SAMPLE INFORMATION

The sample is a Li-Po rechargeable battery (RS Pro, 125-1266) designed to provide reliable power to mobile electronic systems. This flat-shaped battery offers high energy density, making it suitable for lightweight applications. The battery includes electrical terminals, a rolled structure of electrode sheets with a current collector, a pouch casing, and a protective electronic circuit, as shown in Figure 1.B. The battery has a nominal voltage of 3.7 V and a capacity of 2 Ah.

#### B. BATTERY CYCLING AND STATE OF CHARGE MEASUREMENTS

The battery was charged using a protocol called constant-current constant-voltage (CC-CV). A 0.25C C-rate was used for charging and discharging the battery. At this rate, the battery was charged and discharged at 500 mA. During constant-current (CC) mode, a constant electric current was provided to the terminals of the battery. The charging stopped when the voltage reached the safety limit of 4.2 V for this battery. During constant-voltage (CV) mode, the voltage of the battery was held steady at 4.2 V until the current dropped to 50 mA. This last stage marked the battery as fully charged (i.e., 100% SoC).

To discharge the battery, the current was drawn from full to empty capacity. The cell was considered to be fully discharged (i.e., 0% SoC) when the battery reached the safe lower limit of 3 V (Li et al. (2020) and Rahman and Lin (2022)). The battery was charged using a DC power supply (RUIZAO) and discharged using a DC programmable electronic load (Circuit Specialists, CSI3711A). SoC measurements were benchmarked using the OCV method and a 20-minute relaxation time was applied at five different discharge points.

#### C. CONFIGURATION OF EQUIPMENT

For the ultrasound immersion tests, a custom heavy-duty high-speed ultrasonic immersion system (Mistras Group) was connected to an industrial computer with UTwin full-featured ultrasonic C-scan software used for data acquisition, imaging, and analysis. A pulser-receiver (JSR, DPR500) was used to excite a 2.25 MHz focused transducer configured in pulse-echo mode. A fixture was designed and 3D printed to hold the battery in place with the transducer at normal incidence from the surface to generate longitudinal polarised waves. The fixture had screws for levelling, which reduced the chances of mode conversion, where ultrasound waves change characteristics upon interaction with interfaces within the material. The transducer captured the time amplitude measurements using a rectangular scanning pattern, referred to as raster scanning as Figure 2.A shows. A data acquisition card (AD-8xG) registered the high-speed ultrasound information whilst the computer-controlled positioning system with five degrees of freedom (three translational and two rotational) moved the transducer.

#### D. WAVE SPEED AND ATTENUATION MEASUREMENTS

Ultrasound wave speed measurements typically rely on material thickness measurements. Kuo et al. (1990) described a different technique which removes the necessity for inferred material thickness measurements, and Fei et al. (2001) extended this technique to run simultaneous measurements of wave speed and thickness. The absolute attenuation measurements used the equal diffraction approach presented by Yu et al. (2001). These techniques were also adopted by O. Cook et al. (2022) for characterising the porosity in binder jet printed components, and by Jones et al. (2023) to assess the flaws in cold-sintered ZnO. The thickness-independent approach to measure wave speed and attenuation in this study takes inspiration from O. J. Cook et al. (2023) which describes in more detail.

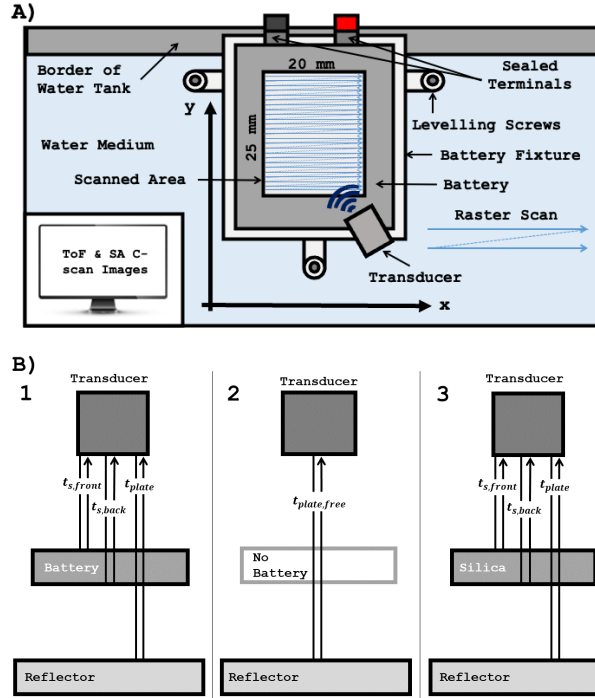


**Figure 2: Raster scans conducted on the battery during the immersion tests (A), and key measurement steps using the thickness-independent approach (B).**

Parts 1 and 2 in Figure 2.B show how the testing is performed. The battery was tested in pulse-echo mode and a reflector was directly located behind the battery. In these tests, the reflector corresponds to the glass surface of the immersion water tank. Time-amplitude measurements were collected at a sampling rate of 500 MHz and 15 ensemble averages to reduce noise effects. The raster scans were conducted in steps of 1 mm for the desired scanning length. With knowledge of the arrival times, the longitudinal wave speed in the battery ( $c_{longitudinal}$ ) was measured using the following formula:

$$c_{longitudinal} = \left[ \frac{t_{plate,free} - t_{plate}}{t_{s,back} - t_{s,front}} + 1 \right] c_{water}, \quad (6)$$

where  $c_{water}$  is the wave speed in the water, and  $t_{s,front}$ ,  $t_{s,back}$ ,  $t_{plate}$ , and  $t_{plate,free}$  are the arrival times for the battery front-surface reflection, battery back-surface reflection, plate surface reflection with the battery present in the propagation path, and plate surface reflection this time when the battery is not present in the propagation path, respectively. Attenuation was given by:

$$\alpha_{sample}(f) = -\frac{1}{2} \ln \left( \frac{|\Gamma_{sample}(f)|(1 - R_{ref}^2)R_{ref}}{|\Gamma_{ref}(f)|(1 - R_{sample}^2)R_{sample}} + \alpha_{water}(f) \frac{(WP_{ref} - WP_{sample})}{t_{sample}} \right), \quad (7)$$

where,  $|\Gamma(f)|$  represents the spectral amplitude of the back surface reflection,  $R$  stands for the reflection coefficient at the interface between the battery or reference silica and the water,  $\alpha_W$  is the attenuation in the water,  $WP$  is the water path,  $t_{sample}$  is the battery material thickness, and subscripts *ref*, *sample*, and *water* refer to reference silica, battery, and water respectively.

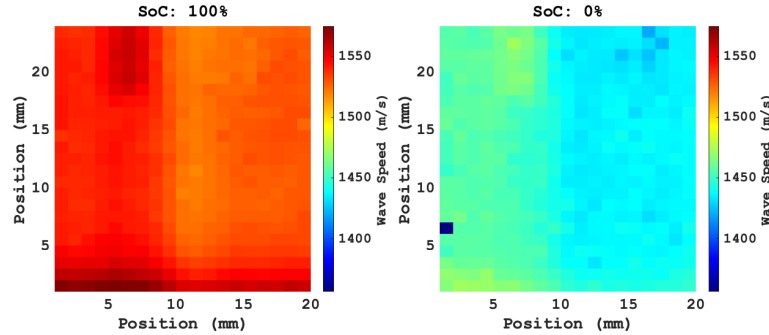


Figure 3: Comparison of wave speeds at full (left) and empty capacity (right).

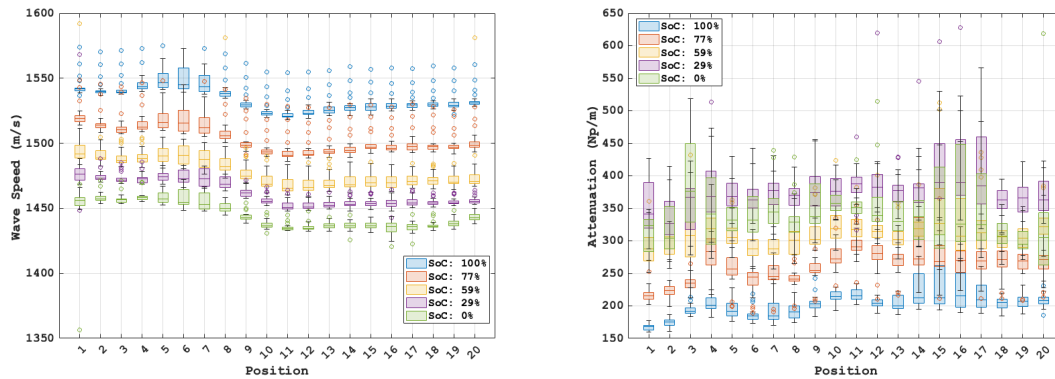


Figure 4: Wave speed and attenuation data processed from C-scans collected at different points in the battery.

#### 4. WAVE SPEED FINDINGS

There is a noticeable shift in wave speed measurements when comparing the battery at full capacity to when it is empty, as Figure 3 shows. The full trend of both wave speed and attenuation measurements from the C-scans are represented in Figure 4. At 100% SoC, the battery shows higher wave speed values on the left region and lower wave speed values on the right region. The current collector is located on the left region of the battery which could indicate higher material stiffness at full charge. The middle part of the battery appears lower in wave speed than the left side. The wave speed slowly increases from the middle region of the battery to the right closer to the edge. The C-scan in Figure 5 clearly shows that the bottom left corner of the battery is also higher in wave speed. Comparing the computed tomography (CT) scans between the bottom left corner and bottom right corner, there appears to be a more pronounced 'void' on the right side of the battery.

As the battery is discharged to 77%, the differences in wave speed appear to be small as Figure 6.A shows. At 77% the material is retaining a relatively modest inhomogeneity in ultrasound measurements. This behaviour indicates that the three key regions of interest (i.e., R1, R2, and R3 as highlighted in Figure 5) remain present. At 77% SoC, the wave speed values drop by approximately 15-35 m/s. When the battery reaches 59% SoC, there seems to be a more pronounced change in wave speeds across the battery. The difference in wave speed between the left and right regions of the battery decreases meaning that the battery starts to show more signs of spatial homogeneity. The left region still maintains higher wave speeds than the right region and the bottom left corner retains higher wave speeds too.

At 29% SoC, both the left and right regions of the battery get closer in wave speed measurements. The wave speeds at the bottom left corner of the battery also tend to decrease. When the battery is fully depleted at 0% SoC, there appears an interesting shift in wave speed properties. Firstly, the wave speed differences



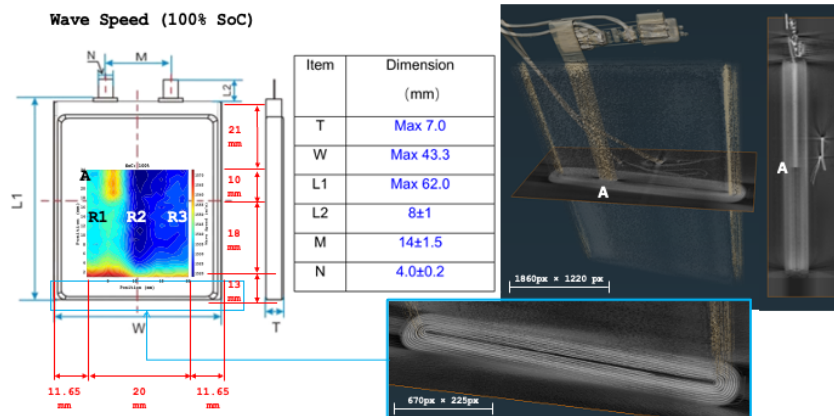


Figure 5: Battery configuration, dimensions, and CT scans of internal structure.

are at their maximum when the battery charge capacity is empty. This means that as the battery discharges, the wave speed decreases. Secondly, observations from the maps indicate that the three main regions of interest drop to almost two. The wave speeds in the middle and right regions of the battery start to merge. The contrast between the left and right regions of the battery is still clear given that the current collecting tab is located. The standard deviations of wave speed across the length of the scanning area of the battery appear higher at 100% SoC than at 0% SoC as shown in Figure 7.A. The standard deviations range between 7 m/s and 8.5 m/s at full capacity compared to the range between 3 m/s and 6 m/s at empty capacity (ignoring the first outlier STD). These measurements show that the battery reaches a more homogeneous level at lower capacity, as observed in the wave speed measurements. Attenuation instead behaves differently as this will be discussed in the next section.

## 5. ATTENUATION FINDINGS

The attenuation measurements of the battery describe the reduction in amplitude of the ultrasound wave as a function of distance through the battery as shown in Figure 6.B. Taking attenuation measurements into account is important as changes can influence the quality of the generated ultrasound images. At full charge, the attenuation through the battery can also be described by the internal structural assembly of the battery. At first, the attenuation measurements appear less steady than the wave speed measurements. The attenuation map also shows the presence of the current collecting tab similar to what was earlier observed in the wave speed measurements. Attenuation appears to be higher in this region and surroundings. The values then tend to decrease when moving towards the middle region and further to the right part of the battery.

At 77% SoC, changes in attenuation are less significant at the bottom and right parts of the battery, while the left side shows the highest changes. As the battery discharges to 59% SoC, attenuation becomes more challenging to interpret, and at 29% SoC, attenuation increases even further. The increased standard deviations at lower SoC confirm this episode as shown in Figure 6.B. There could be something beyond the simple mechanics of the battery impacting these measurements. Previous wave speed measurements demonstrate that the battery reaches more homogeneity at lower SoC levels. The attenuation maps not only increase at lower SoC, but they also become difficult to interpret, which makes it harder to link these with potential SoC inhomogeneities. More tests under different conditions can help explain why these changes are happening, hopefully giving some information about changes due to SoC.

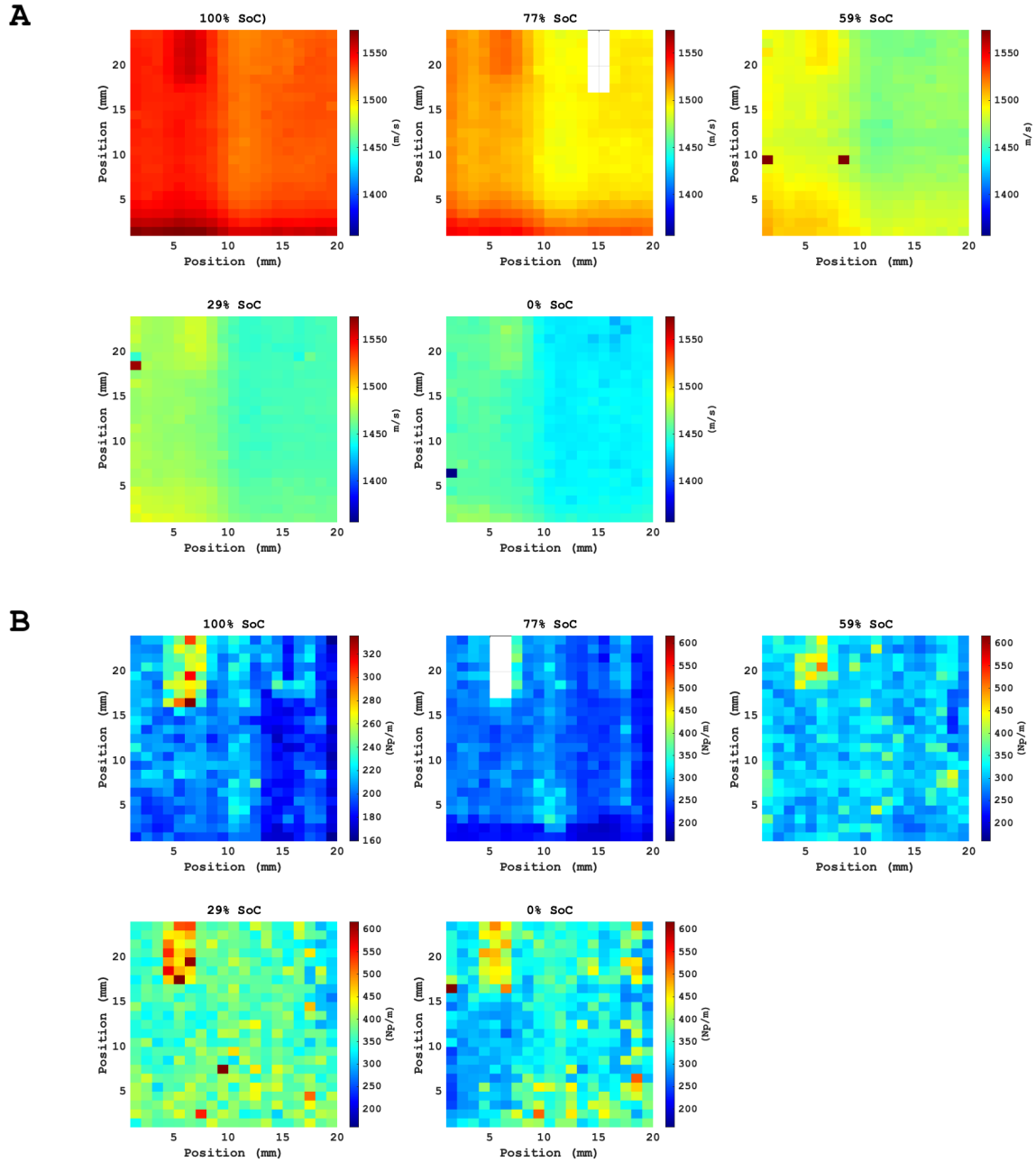


Figure 6: Wave speed (A) and attenuation measurements (B) at different SoC levels.

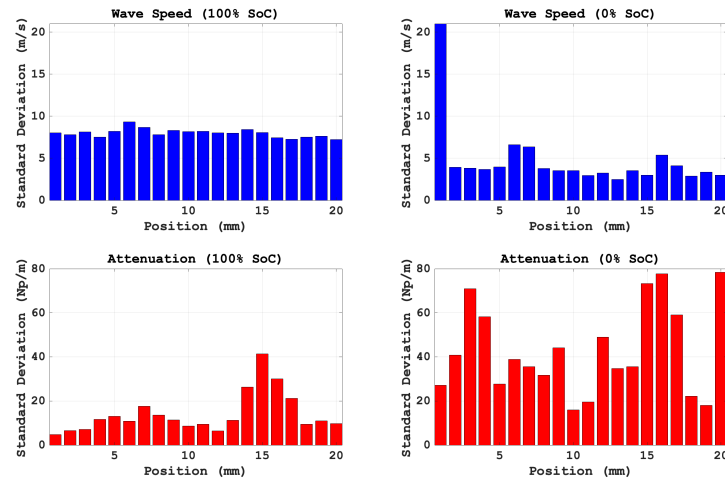


Figure 7: Standard deviations of wave speed (A) and attenuation (B) at full and empty capacity.

## 6. CONCLUSION

Both wave speed and attenuation measurements may prove valuable in assessing the SoC inhomogeneities of Li-Po batteries. This study helped to introduce the use of ultrasound for mapping these acoustic measurements using a thickness-independent approach. Only a portion of the battery surface was raster-scanned during the experiments. Observing a larger surface area would help to evaluate the extreme regions and edge effects on the battery. Applying different C-rates and relaxation periods would provide insights into the impacts of SoC on ultrasound measurements. Quantifying and mapping the inhomogeneities in SoC is the goal for upcoming studies. Future findings will help to reduce over-discharging and/or over-charging as manufacturers can introduce strategies to mitigate these.

## ACKNOWLEDGMENTS

The author would like to extend gratitude to the Argüelles Research Group from the Department of Engineering Science and Mechanics at Pennsylvania State University for hosting this study and providing the necessary equipment, expertise, and resources. Special thanks are directed to Dr Charles Courtney and Dr Christopher Vagg from the Department of Mechanical Engineering at the University of Bath for their invaluable guidance and support throughout this study. Deep appreciation is also extended to the Kube Lab of the Department of Engineering Science and Mechanics at Pennsylvania State University for their collaboration in this research. Furthermore, the author acknowledges the generous grants and funding from the UKRI EPSRC Advanced Automotive Propulsion Systems Centre for Doctoral Training (AAPS CDT), the University of Bath, the Institution of Engineering and Technology (IET), the Institution of Mechanical Engineers (IMechE), the Acoustical Society of America (ASA), and the National Council of Acoustical Consultants (NCAC).

## REFERENCES

Blitz, J., & Simpson, G. (1995). *Ultrasonic methods of non-destructive testing* (Vol. 2). Springer Science & Business Media.

- Braun, A., Wang, H., Funk, T., Seifert, S., & Cairns, E. J. (2010). Depth profile analysis of a cycled lithium ion manganese oxide battery electrode via the valence state of manganese, with soft x-ray emission spectroscopy. *Journal of Power Sources*, *195*(22), 7644–7648.
- Cai, L., An, K., Feng, Z., Liang, C., & Harris, S. J. (2013). In-situ observation of inhomogeneous degradation in large format li-ion cells by neutron diffraction. *Journal of Power Sources*, *236*, 163–168.
- Chueh, W. C., El Gabaly, F., Sugar, J. D., Bartelt, N. C., McDaniel, A. H., Fenton, K. R., Zavadil, K. R., Tyliszczak, T., Lai, W., & McCarty, K. F. (2013). Intercalation pathway in many-particle lifepo4 electrode revealed by nanoscale state-of-charge mapping. *Nano letters*, *13*(3), 866–872.
- Cook, O., Huang, N., Smithson, R., Kube, C., Beese, A., & Argüelles, A. (2022). Ultrasonic characterization of porosity in components made by binder jet additive manufacturing. *Mater. Eval*, *80*, 37–44.
- Cook, O. J., Huang, N., Smithson, R. L., Kube, C. M., Beese, A. M., & Argüelles, A. P. (2023). Uncovering microstructural heterogeneities in binder jet printed ss316l through ultrasonic testing and x-ray computed tomography. *Materials Characterization*, *197*, 112697.
- Davies, G., Knehr, K. W., Van Tassell, B., Hodson, T., Biswas, S., Hsieh, A. G., & Steingart, D. A. (2017). State of charge and state of health estimation using electrochemical acoustic time of flight analysis. *Journal of The Electrochemical Society*, *164*(12), A2746.
- Fang, S., Yan, M., & Hamers, R. J. (2017). Cell design and image analysis for in situ raman mapping of inhomogeneous state-of-charge profiles in lithium-ion batteries. *Journal of Power Sources*, *352*, 18–25.
- Fathoni, G., Widayat, S. A., Topan, P. A., Jalil, A., Cahyadi, A. I., & Wahyunggoro, O. (2017). Comparison of state-of-charge (soc) estimation performance based on three popular methods: Coulomb counting, open circuit voltage, and kalman filter. *2017 2nd International Conference on Automation, Cognitive Science, Optics, Micro Electro-Mechanical System, and Information Technology (ICACOMIT)*, 70–74. <https://doi.org/10.1109/ICACOMIT.2017.8253389>
- Fei, D., Hsu, D. K., & Warchol, M. (2001). Simultaneous velocity, thickness and profile imaging by ultrasonic scan. *Journal of nondestructive evaluation*, *20*, 95–112.
- Ghiji, M., Novozhilov, V., Moinuddin, K., Joseph, P., Burch, I., Suendermann, B., & Gamble, G. (2020). A review of lithium-ion battery fire suppression. *Energies*, *13*(19), 5117.
- Hannan, M. A., Lipu, M. H., Hussain, A., & Mohamed, A. (2017). A review of lithium-ion battery state of charge estimation and management system in electric vehicle applications: Challenges and recommendations. *Renewable and Sustainable Energy Reviews*, *78*, 834–854.
- Hassan, M. K., Hameed, N., Hossain, M. D., Hasnat, M. R., Douglas, G., Pathirana, S., Rahnamayiezekavat, P., & Saha, S. (2023). Fire incidents, trends, and risk mitigation framework of electrical vehicle cars in australia. *Fire*, *6*(8), 325.
- Hsieh, A., Bhadra, S., Hertzberg, B., Gjeltema, P., Goy, A., Fleischer, J. W., & Steingart, D. A. (2015). Electrochemical-acoustic time of flight: In operando correlation of physical dynamics with battery charge and health. *Energy & environmental science*, *8*(5), 1569–1577.
- Hudson, J. A. (1981). Wave speeds and attenuation of elastic waves in material containing cracks. *Geophysical Journal International*, *64*(1), 133–150.
- Hynnen, J., Kumlin, H., & Willstrand, O. (2023). Electric trucks–fire safety aspects.
- Jaguemont, J., Boulon, L., & Dubé, Y. (2016). A comprehensive review of lithium-ion batteries used in hybrid and electric vehicles at cold temperatures. *Applied Energy*, *164*, 99–114.
- Jones, H. N., Trautman, E., Maria, J.-P., Trolier-McKinstry, S., & Argüelles, A. P. (2023). Assessment of flaws in cold sintered zno via acoustic wave speed and attenuation measurements. *Journal of the American Ceramic Society*.
- Kehrwald, D., Shearing, P. R., Brandon, N. P., Sinha, P. K., & Harris, S. J. (2011). Local tortuosity inhomogeneities in a lithium battery composite electrode. *Journal of The Electrochemical Society*, *158*(12), A1393.

- Kuo, I., Hete, B., & Shung, K. (1990). A novel method for the measurement of acoustic speed. *The Journal of the Acoustical Society of America*, 88(4), 1679–1682.
- Lei, J., McLarnon, F., & Kosteki, R. (2005). In situ raman microscopy of individual  $\text{Li}_2\text{O}$  particles in a li-ion battery composite cathode. *The Journal of Physical Chemistry B*, 109(2), 952–957.
- Li, Y., Li, K., Xie, Y., Liu, J., Fu, C., & Liu, B. (2020). Optimized charging of lithium-ion battery for electric vehicles: Adaptive multistage constant current–constant voltage charging strategy. *Renewable energy*, 146, 2688–2699.
- Liao, Z., Zhang, S., Li, K., Zhang, G., & Habetler, T. G. (2019). A survey of methods for monitoring and detecting thermal runaway of lithium-ion batteries. *Journal of Power Sources*, 436, 226879.
- Long, L., Wang, S., Xiao, M., & Meng, Y. (2016). Polymer electrolytes for lithium polymer batteries. *Journal of Materials Chemistry A*, 4(26), 10038–10069.
- Lu, L., Han, X., Li, J., Hua, J., & Ouyang, M. (2013). A review on the key issues for lithium-ion battery management in electric vehicles. *Journal of power sources*, 226, 272–288.
- Maire, P., Evans, A., Kaiser, H., Scheifele, W., & Novák, P. (2008). Colorimetric determination of lithium content in electrodes of lithium-ion batteries. *Journal of The Electrochemical Society*, 155(11), A862.
- Messineo, M. G., Rus, G., Eliçabe, G. E., & Frontini, G. L. (2016). Layered material characterization using ultrasonic transmission. an inverse estimation methodology. *Ultrasonics*, 65, 315–328.
- Migge, S., Sandmann, G., Rahner, D., Dietz, H., & Plieth, W. (2005). Studying lithium intercalation into graphite particles via in situ raman spectroscopy and confocal microscopy. *Journal of Solid State Electrochemistry*, 9, 132–137.
- Mizushima, K., Jones, P., Wiseman, P., & Goodenough, J. B. (1980).  $\text{LiCoO}_2$  ( $0 < x < 1$ ): A new cathode material for batteries of high energy density. *Materials Research Bulletin*, 15(6), 783–789.
- Nanda, J., Remillard, J., O'Neill, A., Bernardi, D., Ro, T., Nietering, K. E., Go, J.-Y., & Miller, T. J. (2011). Local state-of-charge mapping of lithium-ion battery electrodes. *Advanced Functional Materials*, 21(17), 3282–3290.
- Nanekar, P., & Shah, B. (2003). Characterization of material properties by ultrasonics. *BARC Newsletter*, 249, 25–38.
- Padhi, A. K., Nanjundaswamy, K. S., & Goodenough, J. B. (1997). Phospho-olivines as positive-electrode materials for rechargeable lithium batteries. *Journal of the electrochemical society*, 144(4), 1188.
- Rahman, A., & Lin, X. (2022). Li-ion battery individual electrode state of charge and degradation monitoring using battery casing through auto curve matching for standard cccv charging profile. *Applied Energy*, 321, 119367.
- Shao, M. (2014). In situ microscopic studies on the structural and chemical behaviors of lithium-ion battery materials. *Journal of Power Sources*, 270, 475–486.
- Thackeray, M. M., David, W. I., Bruce, P. G., & Goodenough, J. B. (1983). Lithium insertion into manganese spinels. *Materials research bulletin*, 18(4), 461–472.
- Tran, M.-K., Mevawalla, A., Aziz, A., Panchal, S., Xie, Y., & Fowler, M. (2022). A review of lithium-ion battery thermal runaway modeling and diagnosis approaches. *Processes*, 10(6), 1192.
- Wang, J., Li, S., Zhao, Q., Song, C., & Xue, Z. (2021). Structure code for advanced polymer electrolyte in lithium-ion batteries. *Advanced Functional Materials*, 31(12), 2008208.
- Wang, Q., Mao, B., Stoliarov, S. I., & Sun, J. (2019). A review of lithium ion battery failure mechanisms and fire prevention strategies. *Progress in Energy and Combustion Science*, 73, 95–131.
- Xu, B., Lee, J., Kwon, D., Kong, L., & Pecht, M. (2021). Mitigation strategies for li-ion battery thermal runaway: A review. *Renewable and Sustainable Energy Reviews*, 150, 111437.
- Yang, Y., Wang, Z., Jiang, J., Bian, H., Mao, N., & Guo, L. (2020). Effects of different charging and discharging modes on thermal behavior of lithium ion batteries. *Fire and Materials*, 44(1), 90–99.

- Yu, L., Guo, Y., Margetan, F., & Thompson, R. (2001). Effect of microstructure on backwall signal attenuation measurements using focused transducers. *AIP Conference Proceedings*, 557(1), 1330–1337.
- Zhang, R., & Fujimori, S. (2020). The role of transport electrification in global climate change mitigation scenarios. *Environmental Research Letters*, 15(3), 034019.